# Discontinuously propagating waves in the bathoferroin-catalyzed Belousov–Zhabotinsky reaction incorporated into a microemulsion

Alexander A. Cherkashin,[a] Vladimir K. Vanag, and Irving R. Epstein[b]
*Department of Chemistry and Volen Center for Complex Systems, MS 015, Brandeis University, Waltham, Massachusetts 02454, USA*

(Received 17 January 2008; accepted 17 April 2008; published online 29 May 2008)

Three new types of discontinuously propagating waves are reported in the bathoferroin-catalyzed Belousov–Zhabotinsky (BZ) reaction dispersed in water-in-oil Aerosol OT microemulsion. Jumping waves (JWs) are typically observed at or above room temperature and develop from the familiar trigger waves. Bubble waves (BWs) typically emerge from trigger or JWs at similar temperatures, while rotating waves (RWs) evolve from JW at higher temperatures (>40 °C). All these waves propagate discontinuously in a saltatory fashion. Other characteristic features include a discontinuous front for BW consisting of small concentric waves (bubbles) and lateral rotation of annular RWs. All three types of waves, as well as segmented but continuously propagating waves, can coexist. A simple model that is able to describe both jumping and segmented waves is described. © *2008 American Institute of Physics*. [DOI: 10.1063/1.2924119]

## I. INTRODUCTION

The Belousov–Zhabotinsky (BZ) reaction dispersed in water-in-oil Aerosol OT (AOT) microemulsion (ME) (BZ-AOT system) is one of the best prototype systems for studying pattern formation in reaction-diffusion systems. Nonequilibrium structures such as Turing patterns,[1] oscillatory Turing patterns,[2] standing and packet waves,[1,3] oscillons,[4] localized stationary spots,[5] segmented[6,7] and accelerating waves,[1] and antispirals[8] have been found in this system. This rich variety of patterns raises the question as to whether one can control or guide transformations between patterns. Experimental control of spatially extended nonlinear systems with the aid of an external adjustable parameter is an important issue since it allows us to understand complex dynamics better and may have practical applications. For example, the $Ru(bpy)_3$-catalyzed BZ-AOT system is photosensitive and can be controlled by light, which allows the creation of a primitive memory device.[5] Temperature offers another route, which we explore here, to controlling patterns in the BZ-AOT system.

The patterns found in the BZ-AOT system depend on whether the (ME) is above or below its percolation transition. Usually, we observe the stationary Turing patterns [with ferroin or $Ru(bpy)_3$ as catalyst] if a reactive ME is below the percolation transition, while various wave patterns occur if the system is above or in the range of the percolation transition. From a physical point of view, percolation takes place when water droplets, which are isolated in the oil phase at low droplet fraction $\varphi_d$ (=total volume fraction of water and AOT molecules), aggregate into clusters at higher $\varphi_d$ and then, above some threshold, form a net of dynamical water channels that penetrate across the entire ME. The percolation transition is easily detected by monitoring the electrical conductivity, which increases from almost zero (conductivity of pure oil, for example, octane in our case) to the conductivity of saline water. The percolation transition can be induced not only by increasing the droplet fraction[9,10] but also by raising the temperature.[11–14] This observation provides a potential tool for controlling dissipative patterns by changing temperature. We note, however, that an accompanying influence of temperature on the reaction rate constants is inevitable.

In some cases, the percolation transition is quite sharp, occurring over a range of 10° or less.[11,12,15] However, in MEs loaded with the reactants of the BZ reaction, the size of water nanodroplets may have a wider or even a bimodal distribution,[6] leading to a significant broadening of the percolation transition. In Fig. 1, we show typical dependences of conductivity on temperature for the BZ-AOT system at different $\varphi_d$ and a relatively small $\omega \equiv [H_2O]/[AOT]$ ($\omega$ determines the mean radius of the water droplets[16] as $R/\text{nm} \cong 0.17\omega$). In this work, we investigate patterns in the BZ-AOT system catalyzed by bathoferroin.[7] Using this catalyst, we recently found dash waves and segmented spirals.[6,7] The existence of dash waves depends on the presence of two

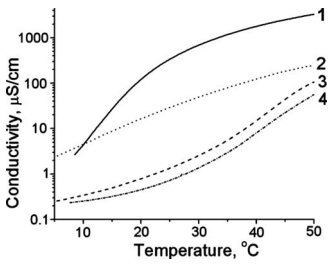


FIG. 1. Temperature dependence of conductivity of AOT MEs. (1) $\omega=15$, $\varphi_d=0.6$; ME is loaded with $[NaBrO_3]=0.18$; (2) $\omega=9$, $\varphi_d=0.5$, $[MA]=0.22M$, $[H_2SO_4]=0.2M$, $[NaBrO_3]=0.18M$, [ferroin]=4 m$M$. (3) $\omega=15$, $\varphi_d=0.5$, $[MA]=0.22M$, $[H_2SO_4]=0.2M$, $[NaBrO_3]=0.18M$, [ferroin] =4 m$M$. (4) $\omega=15$, $\varphi_d=0.35$, water.

[a]Present address: Department of Biophysics, Faculty of Biology, Lomonosov Moscow State University, Moscow 119899, Russia.
[b]Electronic mail: epstein@brandeis.edu.

 

pools of droplets, with radii of ≈2 and ≈20 nm, as detected by quasielastic light scattering.[6,17] The large-radius pool probably consists of clusters of smaller droplets. Temperature can affect the relative populations of these two pools or change the mean cluster size, and thus we expect to find new dynamical behavior as we vary the temperature in the BZ-AOT system.

The emergence of dash waves typically involves an induction period. After mixing the reactants, the familiar trigger waves first appear in the form of concentric circle, spiral, or plane waves. After approximately 1 h, these waves transform into segmented waves. What exactly happens during this induction period is not known, but recent experiments with polyethylene oxide (PEO) added to the BZ-AOT system reveal that PEO, which promotes the formation of large clusters, significantly shortens the induction period and extends the lifetime of the dash waves.[17] Variation in temperature also affects the induction period and makes the emergence of new waves dependent not only on temperature but also on time, a significant parameter in our batch experiments, in which all patterns eventually (after several hours) disappear.

In Sec. II, we describe our methods; in Sec. III, we present the experimental results: in Sec. IV, we introduce a model that generates two qualitatively different types of waves found in our experiments; and in Sec. V, we conclude by discussing our results.

## II. MATERIALS AND METHODS

The BZ reactants [$NaBrO_3$, malonic acid (MA), $H_2SO_4$] were of chemical grade and were used as received. Preparation of MEI, containing malonic acid and $H_2SO_4$, and MEII, containing $NaBrO_3$ and bathoferroin, has been described elsewhere.[6] Bathophenanthroline (4,7-diphenyl-1,10-phenanthroline, Aldrich) (BP) was dissolved in a 1.5*M* solution of AOT in octane to a concentration of 12.3 m*M* with vigorous stirring for 12–24 h. Then, $FeSO_4$ (0.25*M*) was added in the ratio $[BP]/[Fe^{2+}]=3$. In some experiments, bromomalonic acid (BrMA) was added to MEI to reduce the induction period. Bromomalonic acid was prepared by bromination of malonic acid, and in this case, we introduced the following reactants, MA, $H_2SO_4$, $NaBrO_3$, and NaBr, in MEI. Both MEI and MEII had the same values of $\varphi_d$ and $\omega$. The reactive ME was obtained by mixing equal amounts of MEI and MEII.

A small amount (≈0.1 ml) of the reactive ME was sandwiched between two flat windows of thermostated chambers (Fig. 2) separated by a Teflon (Zefluor) membrane spacer (thickness 80 $\mu$m, inner diameter of 25 mm, outer diameter of 47 mm). The two chambers of the reactor were threaded together and had flat glass windows to allow unobscured illumination of the ME from below and observation from above. The chambers were thermostated by continuously flowing water from a temperature-controlled bath. Both chambers were fed from the same water bath, and thus were held at the same temperature. The Zefluor spacer and reactive ME were sandwiched between these chambers. The water fluxes in the chambers did not cause any noticeable mechanical vibrations that might have affected the patterns in the thin layer of reactive ME. The temperature in the reactor could be changed by switching between water fluxes from two water baths, preset at the desired temperature at least 60 min before the experiment (to remove air bubbles).

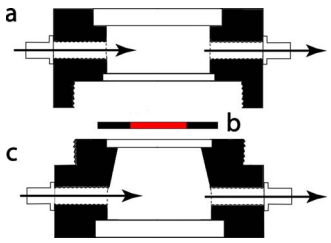


FIG. 2. (Color online) Reactor. (a) and (c) are two thermostated chambers with sealed glass windows; arrows indicate direction of water flux from and to thermostated bath. (b) Teflon spacer between the chambers. The three parts of the reactor are pressed together and the reactive ME (red) is sandwiched between the two glass windows.

Patterns were observed at various temperatures from 10 to 60 °C. The percolation transition, as measured by the electrical conductivity, occurred over a rather wide range of temperature from 10 to 40 °C for our typical conditions of $\varphi_d=0.5-0.6$ and $\omega=15$. Patterns were recorded with a charge coupled device camera mounted on an Olympus-10 stereomicroscope, connected to the frame grabber of a personal computer. IMAGEPRO PLUS software (Media Cybernetics) was used to acquire and to process video sequences. The reactor was illuminated by a slide projector through a 532 nm interference filter (the wavelength corresponding to the absorption maximum of bathoferroin).

Droplet radii were measured with a dynamic light scattering apparatus (DynaPro, Protein Solutions, High Wycombe, U.K.) at room temperature.

## III. RESULTS

*Concentric waves*. Immediately after preparation of the reactive ME by mixing MEI and MEII, we observe conventional circular trigger waves (CW), sometimes referred to as target patterns, continuously propagating from random sites. The velocity of these waves is about 0.8 $\mu$m/s at 10 °C and 8 $\mu$m/s at 40 °C. The outermost wave fronts annihilate upon collision with other waves or with fast phase waves originating from bulk oscillations. The CW can be observed up to several hours at 10–20 °C and for a few minutes at 40–60 °C. With time, the CW become unstable, giving rise to one of the following more complex patterns.

*Jumping waves*. At constant temperature, the CW transform into "jumping waves" (JW), a new class of wave. The term jumping waves has been employed previously to describe propagating fronts in the bromate-sulfite system with an initial *p*H gradient, a phenomenon related to periodic convection,[18] as well as in cardiology to describe the slow and difficult passage of activation fronts from one septal mass to the other through an "intraseptal barrier."[19] We hope that no confusion will arise in our present use of this term. Typical examples of JW are shown in Figs. 3 and 4. In Fig. 3, an ordinary circular wave propagates from a central white spot until a new parallel arc wave suddenly appears a short distance ahead of the original wave front. This new wave

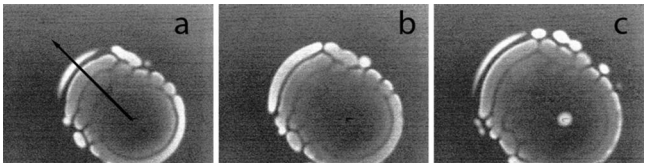


FIG. 3. Jumping waves in the BZ-AOT system ($\omega$=15, $\varphi_d$=0.56$M$, [$BrO_3^-$]=0.18$M$, [MA]=0.3$M$, [$H_2SO_4$]=0.18$M$, [BF]=4.9 m$M$), $T$ =38 °C. Time interval between snapshots (a) and (b) is 10 s, between (b) and (c) is 14 s. Frame size=2.6×2.0 mm$^2$. Arrow in (a) shows the direction of propagation of jumping waves. Normal velocity, $v_n$=16 $\mu$m/s. Wavelength of a jump is 154 $\mu$m.

expands slightly in both the forward and backward directions. Then, the parent wave vanishes, the new wave stops expanding, and generates another parallel front a short distance ahead in the direction of propagation. The new wave fronts continue to jump along the direction of propagation of the original wave; dark separation rings mark the collision lines between successive waves for some time. These waves propagate by discrete jumps, so we refer to them as JWs. The CW-JW transition is considerably accelerated at higher temperatures, while we were unable to find JW at low temperatures (~10 °C). At higher temperatures, the JW become much thinner [see Fig. 4(a)]. JW can coexist with another type of discontinuously propagating wave seen in Fig. 3, bubble waves. We discuss these latter waves in the next subsection.

To characterize the propagation of JW we introduce the following characteristics illustrated in Fig. 4: the wavelength of a jump $\lambda_J$, the wavelength of the wave $\lambda_W$, two periods, $T_W$ and $T_J$, where $T_W$ is the period for generating a new wave

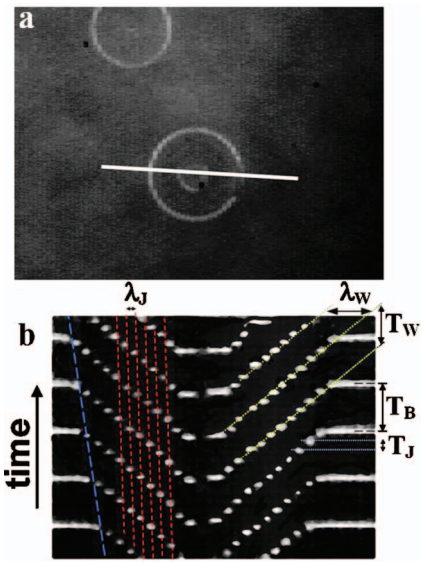


FIG. 4. (Color) Snapshot (a) and space-time plot (b) of jumping waves in the BZ-AOT system at 50 °C. Parameters: $\omega$=15, $\varphi_d$=0.6, [$BrO_3^-$] =0.18$M$, [MA]=0.3$M$, [$H_2SO_4$]=0.2$M$, [BF]=0.0049$M$. The white cross-sectional segment in (a) is 4 mm long. Size of (b), 4 mm×300 s. Velocity of waves, $v_w$=11.8–12.3 $\mu$m/s (slope of yellow-green lines), $v_{shock}$ =1.53 $\mu$m/s (slope of blue line), $v_{shock}=f(T_W,T_B,v_w)=v_w(T_B-T_W)/T_B$ =1.65 $\mu$m/s, $v_{ph\_sh}$=0.34–0.41 $\mu$m/s (phase shift, slope of red lines). Period of bulk oscillations, $T_B$=58 s, period of waves, $T_W$=50 s, period of jumps, $T_J$=11 s. Wavelength of jumps is $\lambda_J=T_J v_w \cong 132$ $\mu$m, and the wavelength of jumping waves is $\lambda_W=T_W v_w \cong 600$ $\mu$m.

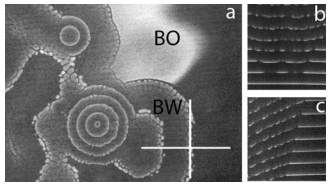


FIG. 5. Bubble waves in the BZ-AOT reaction ($\omega$=15, $\varphi_d$=0.6, [$BrO_3^-$] =0.213$M$, [MA]=0.3$M$, [$H_2SO_4$]=0.3$M$, [NaBr]=0.067, [BF]=4.9 m$M$, (MA):[BrMA]=1:1). The snapshot was taken 50 min after preparation of the reactive ME. $T$=30 °C. Size=(a) 7.9×5.9 mm$^2$, (b) 2.6 mm ×19.3 min, (c) 3 mm×25 min. Space-time plots are made along the straight lines shown in (a) as white horizontal ((b), length 3.0 mm) and vertical [(c), length of 2.6 mm] bars. Time vector in (b) and (c) is directed from the bottom to the top of the figure. Time axes in (b) and (c) are not matched. BO—bulk oscillations; BW—bubble wave. Period of bulk oscillations, $T_B$=158 s, period of waves, $T_W$=150 s. Period of jumps, $T_J$ =31.4 s, wavelength of jumps $\lambda_J=T_J v_W \cong 104$ $\mu$m, where $v_w$=3.3 $\mu$m/s and the wavelength of bubble waves is $\lambda_W=T_W v_W$=495 $\mu$m.

from a pacemaker, and $T_J$ is the period of jumps of a single wave; $\lambda_J=T_J v_W$, and $\lambda_W=T_W v_W$, where $v_W$ is the velocity of JWs. Usually, the wavelength of a jump is between 100 and 250 $\mu$m. In most cases, $\lambda_W \gg \lambda_J$ ($\lambda_J/\lambda_W \cong 0.2$, for Fig. 4). In some cases, JW coexist with bulk oscillations (period $T_B$). In this case, if $T_B > T_W$, a shock point exists, where JW collide with a fast phase wave. This point propagates in space at velocity $v_{shock}=v_W(T_B-T_W)/T_B$. The space-time plot [Fig. 4(b)] illustrates how to calculate $\lambda_J$, $\lambda_W$, $T_J$, $T_W$, $T_B$, and $v_W$, $v_{ph\_sh}$, and $v_{shock}$. A set of parallel red dotted lines plotted across the adjacent "jumps" of consecutive waves suggests some "memory" features: the next wave "remembers" the position of the previous wave, resulting in a phase shift that can be calculated as $v_{ph\_sh}T_W/\lambda_J$ (≅0.14). In some cases, e.g., the JW shown in Fig. 3, the phase shift is about 0.5, making the JW similar but not identical to standing waves.

*Bubble waves*. These are similar to JW in the discontinuous character of their propagation. However, unlike CW and JW, BW are composed of discrete spots or "bubbles" (Fig. 5). BWs usually evolve in time from JW or CW via disruption or incomplete closure of wave fronts. When several small segments appear close to each other along the wave front, the latter consists of numerous spots. When BW first emerge from JW, they typically move along the direction of propagation of the parent front as a set of jumping spots but do not spread in the lateral direction. Later, the BW begin to extend in the lateral direction as well, so that they eventually occupy the entire periphery of the circular wave front and can even fuse with wave fronts from the other centers to create more complex front lines [Fig. 5(a)].

In Fig. 5(a), we see two wave centers that generate CW. At some distance from the center, the usual trigger waves transform into BW, which die upon collision with a fast phase wave of bulk oscillations (BOs). The circular waves almost always transform to more complex patterns due to fusion of fronts originating from different pacemakers. Figures 5(b) and 5(c) show the space-time plots along the lateral and normal directions of a set of BW. In Fig. 5(b), we see how the continuous wave front breaks up into a discontinuous front, composed of spots with decreasing diameter. In the normal direction, BW propagate discontinuously [Fig. 5(c)], like JW. The small bubbles are small circular waves that

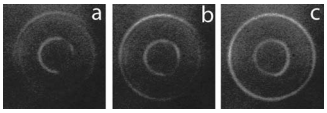


FIG. 6. Rotating waves in the BZ-AOT system at 50 °C. Parameters: $\omega=15$, $\varphi_d=0.6$, $[BrO_3^-]=0.18M$, $[MA]=0.3M$, $[H_2SO_4]=0.2M$, $[BF]=0.0049M$. Size of snapshots is $3\times3$ mm$^2$. Time between snapshots (a) and (b) is 1 s and between (b) and (c) is 2 s.

propagate for a short distance in all directions with the same velocity, approximately equal to the velocity of the total wave front, $v_W$(3.3–4 $\mu$m/s). The characteristic size of the bubbles, $\lambda_b$ ($\cong$80–100 $\mu$m), is slightly smaller than the size of a jump $\lambda_J$ ($\cong$100–120 $\mu$m).

*Rotating waves*. These RW (Fig. 6) are a variant of jumping waves. These waves[20] give the impression of wave rotation, a front circulating around the circumference of a circle. This sense comes from the very high normal wave velocity, $v_n$ (60 $\mu$m/s for RW versus 12 $\mu$m/s for JW at 50 °C or even 3–5 $\mu$m/s at lower temperatures), and slow lateral propagation speed $v_1$ (15–40 $\mu$m/s at 50 °C). For RW, $v_n/v_1>1$ (or even $\gg1$), while for JW, $v_n/v_1\ll1$. RW typically occur at high temperatures (above 40 °C) and develop from JWs. BWs also can transform into RWs, if the temperature is increased in the course of the experiment. As shown in Fig. 6, new fronts appear as incomplete segments of a circular wavefront [Fig. 6(a)] and move laterally to close the circle [Figs. 6(b) and 6(c)]. This lateral propagation is a form of phase wave. On occasion, a few successive rotating fronts of RWs can be observed simultaneously, giving the impression of a rotating wheel.

We saw in Fig. 3 that JW and BW can coexist. Figure 5 shows that CW and BW also can coexist. More surprisingly, JWs, BWs, and the segmented waves (SWs) described elsewhere[7] can also coexist (see Fig. 7). SWs also evolve from the usual concentric trigger waves. The velocity of SWs is slightly smaller than that of JWs. Collision of all types of waves leads to their annihilation. Note that SWs propagate continuously, while JWs, BWs, and RWs propagate discontinuously in the radial direction (by jumps). The coexistence of these essentially different types of waves imposes strict requirements on any theoretical model of these phenomena.

Before they disappear in our batch experiment, all types of waves, JWs, BWs, and RWs, transform into irregular waves. The higher the temperature, the faster this transition to chaotic waves.

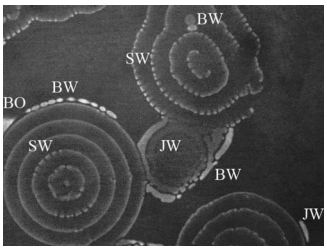


FIG. 7. Three types of waves, segmented waves (SWs), jumping waves (JWs), and bubble waves (BWs) can coexist. Parameters of the BZ-AOT system: $\omega=15$, $\varphi_d=0.6$, $[BrO_3^-]=0.18M$, $[MA]=0.3M$, $[H_2SO_4]=0.18M$, $[BF]=4.9$ m$M$, $T=40$ °C. Snapshot was taken 50 min after preparation of reactive ME. The frame size is $7.9\times5.9$ mm$^2$.

## IV. THEORETICAL SECTION

Jumping, bubble, and rotating waves have not previously been observed in experimental reaction-diffusion systems. All these waves propagate in the normal direction in a saltatory manner. Reviewing different models and ideas that might be useful in explaining such waves, we noticed that the model proposed by Purwins' group[21,22] can explain two types of wave behavior: moving localized wave segments, which are similar to our continuous segmented waves, and jumping solitary waves, which are similar to our jumping waves.[23] This model consists of a FitzHugh–Nagumo core (equations for an activator $u$ and an inhibitor $v$) augmented with a third variable, a second, fast-diffusing inhibitor $w$ coupled to the activator $u$,

$$\partial u/\partial t = \alpha u - u^3 - k_3 v - k_4 w - k_1 + D_u \Delta u, \tag{1}$$

$$\partial v/\partial t = (u - v)/\varepsilon_1 + D_v \Delta v, \tag{2}$$

$$\partial w/\partial t = u - w + D_w \Delta w. \tag{3}$$

In the BZ-AOT system, $u$ can be associated with the activator species $HBrO_2$, while $v$ and $w$ can be taken to represent the inhibitors $Br^-$ (water soluble) and $Br_2$ (oil soluble).

In general, models (1)–(3) may have two stationary steady states (SS), but here we investigated parameters where only a single stable SS occurs. We previously showed[6] that one can generate dash waves if the system has two SS, one of which, SSI, is excitable and responsible for wave propagation, while the second, SSII, is Turing unstable and is responsible for segmentation of the wave. The system switches from SSI to SSII in a narrow region corresponding to passage of the wavefront.

The combination of excitability and Turing instability can also be realized for a single SS. For example, in models (1)–(3), Eqs. (1) and (2) can produce excitability and wave propagation, while the fast-diffusing inhibitor $w$ can add subcritical Turing instability to the full system (1)–(3). An important feature of system (1)–(3) is that it can be in a regime of subcritical wave instability as well.[24] Like Turing instability, wave instability provides a system with a characteristic wavelength. A subcritical wave instability may result in jumping waves in two dimensions, which are analogous to the jumping oscillons found in one dimension.[23] Its ability to support at least two wave regimes, i.e., jumping waves and segmented continuous waves, as well as instability between two or more wave regimes, like jumping waves and continuously propagating waves,[23] makes system (1)–(3) an attractive candidate to model the phenomena of interest here.

For simulation of reaction-diffusion system (1)–(3), we employ the FLEXPDE package,[25] in which a Newton–Raphson iteration process is used with a variable time step and mesh. FLEXPDE refines the triangular finite element mesh and/or time step until the estimated error in any variable is less than a specified tolerance, which we choose as small as $10^{-3}$.

To limit the number of adjustable parameters, we fix $k_1=8.5$, $k_3=10$, $k_4=2$, $\varepsilon_1=50$, and $D_w=1$ and vary only $\alpha$, $D_u$, and $D_v$. An example of jumping waves in model (1)–(3) is shown in Fig. 8(a)–8(c). The space-time plot in Fig. 8(d) is

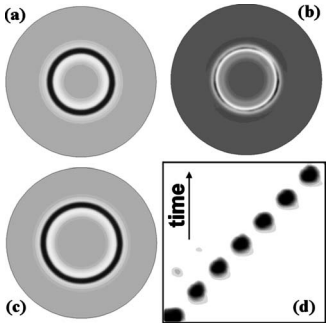


FIG. 8. $u$-maps of jumping circular waves in models (1)–(3) at $\alpha=2$, $k_1=8.5$, $k_3=10$, $k_4=2$, $\varepsilon_1=50$, $D_u=0.03$, $D_v=0.01$, and $D_w=1$. The radius in snapshots (a)–(c) is 15, times of snapshots=(a) 39, (b) 42, and (c) 48. (d) Space-time plot along a radius. At $t=0$, a small central area was perturbed. Size of (d): space=10 (left edge corresponds to center of the circular area), total time=60.

analogous to that in Fig. 4(b), except that here we are in the nonoscillatory regime and observe only a single jumping wave (an oscillatory pacemaker for JW is also possible in this model[23]). From Fig. 8(d), we can extract such characteristics of the JW as the velocity, $v_W(\cong 0.158)$, wavelength of a jump, $\lambda_J(\cong 1.4)$, and period of a jump, $T_J$ $(\cong 8.81)$.

Small changes in parameters ($\alpha=3$, $D_u=D_v=0.08$) allowed us to find segmented continuously propagating waves in models (1)–(3), shown in Fig. 9. In this computer experiment, a small central area was initially perturbed, then the perturbed region split into two pulses propagating in the opposite directions. The ends of these two pulses generated small segmented waves propagating toward the periphery. The velocity of these SW is $v\cong 0.093$, which is smaller than $v_W$ in the previous example, despite the fact that $\alpha$ (the rate of autocatalysis) and $D_u$ (diffusion coefficient of activator) are larger. This indicates that a simple relation for the velocity of trigger waves of the form $v\cong(\alpha D_u)^{1/2}$ does not hold in this system. Note that in our experiment, SWs also move more slowly than JWs.

## V. DISCUSSION

The bathoferroin-catalyzed BZ-AOT system demonstrates a wide variety of wave patterns, including conventional trigger waves and segmented waves that propagate continuously, and jumping waves, bubble waves, and rotating waves that propagate discontinuously. Different waves, for example, such pairs as CW-JW, JW-BW, BW-SW, and JW-SW, can coexist and compete with each other. Figure 10 schematically illustrates the transformations we have observed between the various types of wave patterns. We have shown that transitions between different types of waves are promoted and accelerated by temperature, but at this stage, we cannot say whether these transitions are induced by structural changes in the ME or by the accelerated chemical kinetics of the BZ reaction.

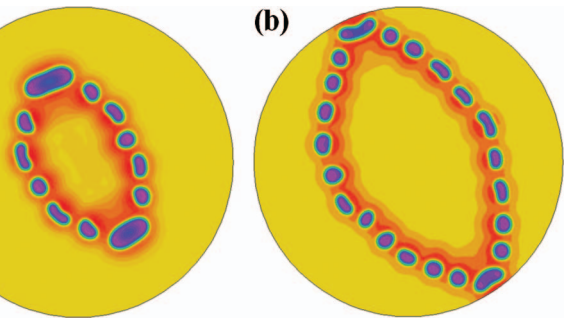


FIG. 9. (Color) Continuously propagating segmented waves in models (1)–(3) at $\alpha=3$, $k_1=8.5$, $k_3=10$, $k_4=2$, $\varepsilon_1=50$, $D_u=D_v=0.08$, $D_w=1$. $t=$(a) 40 and (b) 65. The radius of the domain is 12. At $t=0$, a small central area was perturbed.

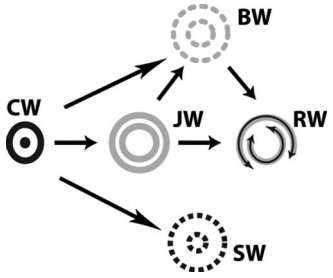


FIG. 10. Transformations of wave patterns in bathoferroin-catalyzed BZ-AOT system: CWs, continuous trigger waves; SWs, segmented waves; JWs, jumping waves; BWs, bubble waves; and RWs, rotating waves. JW, BW, and RW are discontinuously propagating waves, while SW propagate smoothly.

The discontinuously propagating waves found here have never been observed in the classical aqueous BZ reaction and probably require a water-in-oil ME or some other microstructured medium. The configuration studied here provides the BZ-AOT system with two sufficiently different diffusion coefficients $D_i$, with small $D_1$ for water-soluble species (for example, activator $HBrO_2$ and inhibitor $Br^-$) and large $D_2$ for oil-soluble species like the inhibitor $Br_2$. Using the simple models (1)–(3), we were able to simulate two essentially different types of waves, continuously and discontinuously propagating. However, a more detailed model or a different set of parameters of models (1)–(3) will be needed to simulate coexistence of these two types of waves.

Sometimes, an analogy between two apparently unrelated phenomena can shed light on the mechanism of the less well understood phenomenon. We suggest a parallel between the segmented and jumping waves found in these experiments and the translational and nontranslational motion of perturbed Turing patterns seen in our theoretical studies.[26] In the latter computer experiments, one parameter of the photosensitive Lengyel–Epstein model[27–29] is adjusted in such a way as to allow Turing patterns to occur only in a narrow stripe (the mask), which can be moved perpendicular to its long axis. In the rest of the system, Turing patterns cannot arise. If the mask is stationary, we obtain a one-dimensional (1D) Turing pattern, spots, or a single stripe depending on the parameters of the model, along the mask. If the mask moves slowly, we have continuous translational motion of the 1D Turing patterns with the mask. An analogous result was experimentally obtained.[30] If the Turing pattern consists of spots, this behavior is analogous to SW. If the mask velocity is increased above a threshold, nontranslational motion of the Turing pattern occurs. In Fig. 11, we show this nontranslational motion of a single stripe, a phenomenon analogous to jumping waves.

FIG. 11. Four consecutive snapshots of Turing patterns (narrow black stripes) moving nontranslationally at constant velocity (=2) of the up-moving mask (the mask is not shown). The width of the mask (=4.5) is slightly larger than the width of a single black stripe. Time between snapshots is 1. Horizontal size of snapshots is 30. Turing instability occurs only in the shadow of the mask.

In the case of the moving mask, the velocity of the mask can be varied independently of the other parameters. In JW or SW, the velocity of the waves can, in general, depend on the shape of the wave patterns or on the manner of wave propagation. These are clearly more complex phenomena. Nonetheless, the notion that propagating wave activity can switch the system into a new Turing unstable state in a narrow moving zone may hold the key to both SW and JW.

## ACKNOWLEDGMENTS

This work was supported, in part, by the Chemistry Division of the National Science Foundation through Grant Nos. CHE-0615507 and CHE-0526866, by the donors of the American Chemical Society Petroleum Research Fund through Grant No. 42222-AC6, and by the Russian Foundation for Basic Research through Grant No. 07-04-00278-a.

[1] V. K. Vanag and I. R. Epstein, Phys. Rev. Lett. **87**, 228301 (2001).
[2] A. Kaminaga, V. K. Vanag, and I. R. Epstein, J. Chem. Phys. **122**, 174706 (2005).
[3] V. K. Vanag and I. R. Epstein, Phys. Rev. Lett. **88**, 088303 (2002).
[4] V. K. Vanag and I. R. Epstein, Phys. Rev. Lett. **92**, 128301 (2004).
[5] A. Kaminaga, V. K. Vanag, and I. R. Epstein, Angew. Chem., Int. Ed. **45**, 3087 (2006).
[6] V. K. Vanag and I. R. Epstein, Phys. Rev. Lett. **90**, 098301 (2003).
[7] V. K. Vanag and I. R. Epstein, Proc. Natl. Acad. Sci. U.S.A. **100**, 14635 (2003).
[8] V. K. Vanag and I. R. Epstein, Science **294**, 835 (2001).
[9] M. Lagues, R. Ober, and C. Taupin, J. Phys. (Paris), Lett. **39**, L487 (1978).
[10] C. Boned, J. Peyrelasse, and Z. Saidi, Phys. Rev. E **47**, 468 (1993).
[11] L. Schlicht, J. H. Spilgies, F. Runge, S. Lipgens, S. Boyce, D. Schubel, and G. Ilgenfritz, Biophys. Chem. **58**, 39 (1996).
[12] H. Kataoka, T. Eguchi, H. Masui, K. Miyakubo, H. Nakayama, and N. Nakamura, J. Phys. Chem. B **107**, 12542 (2003).
[13] Y. Feldman, N. Kozlovich, I. Nir, N. Garti, V. Archipov, and V. Fedotov, J. Phys. Chem. **100**, 3745 (1996).
[14] Y. Feldman, N. Kozlovich, I. Nir, and N. Garti, Phys. Rev. E **51**, 478 (1995).
[15] S. K. Mehta and S. Sharma, J. Colloid Interface Sci. **296**, 690 (2006).
[16] M. Kotlarchyk, S. H. Chen, and J. S. Huang, J. Phys. Chem. **86**, 3273 (1982).
[17] J. Carballido-Landeira, I. Berenstein, P. Taboada, V. Mosquera, V. K. Vanag, I. R. Epstein, V. Pérez-Villar, and A. P. Muñuzuri, Phys. Chem. Chem. Phys. **10**, 1094 (2008).
[18] I. P. Nagy, A. Keresztessy, and J. A. Pojman, J. Phys. Chem. **99**, 5385 (1995).
[19] G. A. Medrano, A. De Micheli, and P. Iturralde, Acta Cardiol. **55**, 283 (2000).
[20] See EPAPS Document No. E-JCPSA6-128-018821 for a movie of rotating waves in the bathoferroin-catalyzed BZ-AOT system. Parameters: $\omega=15$, $\varphi_d=0.6$, $[BrO_3^-]=0.18M$, $[MA]=0.3M$, $[H_2SO_4]=0.2M$, $[BF]=0.0049M$, $T=50$ °C. Frame size is $3.9\times3.7$ mm$^2$. Total real time of the movie is 70 s. For more information on EPAPS, see http://www.aip.org/pubservs/epaps.html.
[21] M. Bode, A. W. Liehr, C. P. Schenk, and H.-G. Purwins, Physica D **161**, 45 (2002).
[22] C. P. Schenk, M. Or-Guil, M. Bode, and H.-G. Purwins, Phys. Rev. Lett. **78**, 3781 (1997).
[23] L. F. Yang, A. M. Zhabotinsky, and I. R. Epstein, Phys. Chem. Chem. Phys. **8**, 4647 (2006).
[24] V. K. Vanag and I. R. Epstein, Chaos **17**, 037110 (2007).
[25] FLEXPDE (http://www.pdesolutions.com).
[26] V. K. Vanag and I. R. Epstein, Phys. Rev. E **67**, 066219 (2003).
[27] M. Dolnik, I. Berenstein, A. M. Zhabotinsky, and I. R. Epstein, Phys. Rev. Lett. **87**, 238301 (2001).
[28] A. K. Horváth, M. Dolnik, A. P. Muñuzuri, A. M. Zhabotinsky, and I. R. Epstein, Phys. Rev. Lett. **83**, 2950 (1999).
[29] I. Lengyel and I. R. Epstein, Science **251**, 650 (1991).
[30] D. G. Míguez, V. Pérez-Villar, and A. P. Muñuzuri, Phys. Rev. E **71**, 066217 (2005).